The PANS and PITM model: a new formulation of f_k

***L. Davidson*[1], *C. Friess*[2]**

[1] ***Div. of Fluid Dynamics***
Dept. of Mechanics and Maritime Sciences (M2)
Chalmers University of Technology, Gothenburg, Sweden
[2] ***Aix-Marseille Université, CNRS, Centrale Marseille***
M2P2 UMR 7340, 13451, Marseille, France

lada@chalmers.se

Abstract

The partially averaged Navier-Stokes (PANS) model, proposed in Girimaji (2006), can be used to simulate turbulent flows either as a RANS, LES or DNS. The Partially Integrated Transport Model (PITM) is identical to PANS except that in PANS the diffusion coefficients in the k and ε are modified. Both models include f_k which denotes the ratio of modeled to total kinetic energy. In RANS, $f_k = 1$, and in DNS it goes to zero. In the present study we propose a new formulation for f_k based on the H-equivalence introduced by Friess *et al.* (2015).

1 Introduction

The PANS model was proposed by Girimaji (2006) and the PITM was proposed by Schiestel & Dejoan (2005), Chaouat & Schiestel (2005). The critical parameter in both models is f_k (it is called r in PITM). It is defined as the ratio of the modeled to the total turbulent kinetic energy. Several proposals have been made on how to compute it. One way to compute f_k is as proposed by Basara et al. (2011)

$$f_k = C_\mu^{-1/2}\left(\frac{\Delta}{L_t}\right)^{2/3}, L_t = \frac{k_{tot}^{3/2}}{\varepsilon} \qquad (1)$$

where $\Delta = (\Delta V)^{1/3}$. Kenjeres & Hanjalic (2006) have made a slightly different proposal which reads

$$f_k = \frac{\Delta}{L_t} \qquad (2)$$

Another way is to compute f_k from its definition, i.e.

$$f_k = \frac{k}{k_{tot}} \qquad (3)$$

where k_{tot} is computed using the running average. Other formulations were proposed by Girimaji & Abdol-Hamid (2005) who compute it as $3(\Delta_{min}/L_t)^{2/3}$ where Δ_{min} is the smallest grid cell size and $L_t = k_{tot}^{3/2}/\varepsilon$. Foroutan & Yavuzkurt (2014) derives an expression from the energy spectrum which reads

$$f_k = 1 - \left[\frac{(\Lambda/\Delta)^{2/3}}{0.23 + (\Lambda/\Delta)^{2/3}}\right]^{9/2} \qquad (4)$$

In Davidson (2016), the expression in Eq. 2 was found to give far too small f_k. The form in Eq. 1 and 3 were evaluated but it was found that a constant $f_k = 0.4$ in the LES region is superior.

The present paper is based on the work in Friess et al. (2015) where they derived a relation between DES and PITM. They showed that the DES model could be formulated using f_k. They call this model an equivalent DES model. The relation between DES and PITM/PANS is used in the present work, but it is used the other way around: a new form of f_k is derived based on the DES model.

2 The PANS and PITM Model

The low-Reynolds number Partially-Averaged Navier-Stokes (LRN PANS) turbulence model reads

$$\frac{dk}{dt} = \frac{\partial}{\partial x_j}\left[\left(\nu + \frac{\nu_t}{\sigma_{ku}}\right)\frac{\partial k}{\partial x_j}\right] + P_k - \varepsilon \qquad (5)$$

$$\frac{d\varepsilon}{dt} = \frac{\partial}{\partial x_j}\left[\left(\nu + \frac{\nu_t}{\sigma_{\varepsilon u}}\right)\frac{\partial \varepsilon}{\partial x_j}\right] + C_{\varepsilon 1}P_k\frac{\varepsilon}{k} - C_{\varepsilon 2}^*\frac{\varepsilon^2}{k}$$

$$\nu_t = C_\mu f_\mu \frac{k^2}{\varepsilon}, P_k = 2\nu_t \bar{s}_{ij}\bar{s}_{ij}, \bar{s}_{ij} = \frac{1}{2}\left(\frac{\partial \bar{v}_i}{\partial x_j} + \frac{\partial \bar{v}_j}{\partial x_i}\right)$$

$$C_{\varepsilon 2}^* = C_{\varepsilon 1} + \frac{f_k}{f_\varepsilon}(C_{\varepsilon 2}f_2 - C_{\varepsilon 1}), \sigma_{ku} \equiv \sigma_k\frac{f_k^2}{f_\varepsilon}, \sigma_{\varepsilon u} \equiv \sigma_\varepsilon\frac{f_k^2}{f_\varepsilon}$$

$$\sigma_k = 1.4, \sigma_\varepsilon = 1.4, C_{\varepsilon 1} = 1.5, C_{\varepsilon 2} = 1.9, C_\mu = 0.09$$

where $d/dt = \partial/\partial t + \bar{v}_j \partial/\partial x_j$ denotes the material derivative. The damping functions are given by

$$f_2 = \left[1 - \exp\Big(-\frac{y^*}{3.1}\Big)\right]^2 \left\{1 - 0.3\exp\Big[-\Big(\frac{R_t}{6.5}\Big)^2\Big]\right\}$$

$$f_\mu = \left[1 - \exp\Big(-\frac{y^*}{14}\Big)\right]^2 \left\{1 + \frac{5}{R_t^{3/4}}\exp\Big[-\Big(\frac{R_t}{200}\Big)^2\Big]\right\}$$

$$R_t = \frac{k^2}{\nu\varepsilon}, \quad y^* = \frac{U_\varepsilon y}{\nu}, \quad U_\varepsilon = (\varepsilon\nu)^{1/4} \tag{6}$$

The functions $f_k = k/(k + k_{res})$ and f_ε denote the ratio of modeled to total kinetic energy and modeled to total dissipation, respectively. For high Reynolds numbers (as in the present work), the dissipation is modeled which means that $f_\varepsilon = 1$. In the PITM model, we set $\sigma_{ku} \equiv \sigma_k$ and $\sigma_{\varepsilon u} \equiv \sigma_\varepsilon$.

f_k derived from the equivalence criterion

In Friess et al. (2015) a relation between f_k and the grid step is derived, through the establishment of a statistical equivalence between DES and PITM. To that aim, they performed perturbation analyses about the equilibrium states, representing small variation of the energy partition. They did the analysis with and without considering inhomogeneity. That derivation is summarized here in a homogeneous framework. Let us first consider the PANS/PITM equations. For equilibrium turbulence $d\tau/dt = 0$ where $\tau = k/\varepsilon$, Eq. 5 gives

$$\begin{aligned}\frac{d\tau}{dt} &= \frac{1}{\varepsilon}\frac{dk}{dt} - \frac{k}{\varepsilon^2}\frac{d\varepsilon}{dt} = \frac{1}{\varepsilon}\left(P^k + D^k - \varepsilon\right) \\ &- \frac{k}{\varepsilon^2}\left(C_{\varepsilon 1}\frac{\varepsilon}{k}P^k + D^\varepsilon - C^*_{\varepsilon 2}\frac{\varepsilon^2}{k}\right) = 0\end{aligned} \tag{7}$$

where D^k and D^ε denote the diffusion term for k and ε, respectively. For local homogeneous turbulence (i.e. $D^k = D^\varepsilon = 0$), it can be written

$$\begin{aligned}\gamma(C_{\varepsilon 1} - 1)Sk &= (C^*_{\varepsilon 2} - 1)\varepsilon \\ \gamma = \frac{P^k}{Sk}, S &= (2\bar{s}_{ij}\bar{s}_{ij})^{1/2}\end{aligned} \tag{8}$$

The quantities that are affected by the partition between modeled and resolved turbulence (i.e. f_k) in Eq. 8 are γ, S, k and $C^*_{\varepsilon 2}$.[1] Differentiation gives

$$\delta\gamma Sk + \delta S\gamma k + \delta k\gamma S = \frac{\delta C^*_{\varepsilon 2}\varepsilon}{C_{\varepsilon 1} - 1} \tag{9}$$

so that

$$\frac{\delta\gamma}{\gamma} + \frac{\delta S}{S} + \frac{\delta k}{k} = \frac{\delta C^*_{\varepsilon 2}\varepsilon}{(C_{\varepsilon 1} - 1)\gamma Sk} = \frac{\delta C^*_{\varepsilon 2}}{C^*_{\varepsilon 2} - 1} \tag{10}$$

Equation 10 was derived for the PANS/PITM equations. Now we repeat the derivation for the DES equations. The differences between DES and PITM/PANS are that in DES (i) $C^*_{\varepsilon 2} = C_{\varepsilon 2}$ is constant and (ii) the dissipation term in the equation for modeled energy k is replaced with $\psi\varepsilon$, where $\psi = \max\left(1, \frac{k^{3/2}/\varepsilon}{C_{DES}\Delta}\right)$

$$\frac{dk}{dt} = \frac{\partial}{\partial x_j}\left[\left(\nu + \frac{\nu_t}{\sigma_k}\right)\frac{\partial k}{\partial x_j}\right] + P_k - \psi\varepsilon \tag{11}$$

$$\frac{d\varepsilon}{dt} = \frac{\partial}{\partial x_j}\left[\left(\nu + \frac{\nu_t}{\sigma_\varepsilon}\right)\frac{\partial \varepsilon}{\partial x_j}\right] + C_{\varepsilon 1}P_k\frac{\varepsilon}{k} - C_{\varepsilon 2}\frac{\varepsilon^2}{k}$$

Assuming $d\tau/dt = 0$ and local homogeneous turbulence gives

$$\gamma(C_{\varepsilon 1} - 1)Sk = (C_{\varepsilon 2} - \psi)\varepsilon \tag{12}$$

We differentiate so that

$$\frac{\delta\gamma}{\gamma} + \frac{\delta S}{S} + \frac{\delta k}{k} = -\frac{d\psi\varepsilon}{(C_{\varepsilon 1} - 1)Sk\gamma} = -\frac{d\psi}{C_{\varepsilon 2} - \psi} \tag{13}$$

Equations 9 and 13 describe how $C^*_{\varepsilon 2}$ and ψ depend on variations in γ, S and k. The parameters $C^*_{\varepsilon 2}$ and ψ vary from $C_{\varepsilon 2}$ and 1 (RANS values), respectively, to $C^*_{\varepsilon 2}$ and $\psi(\Delta)$ (LES values). Combining Eqs. 9 and 13 and integrating from RANS to LES conditions ($C^*_{\varepsilon 2}$ and ψ)

$$\begin{aligned}\int_{C_{\varepsilon 2}}^{C^*_{\varepsilon 2}} \frac{dC^*_{\varepsilon 2}}{C^*_{\varepsilon 2} - 1} &= \int_1^\psi -\frac{d\psi}{C_{\varepsilon 2} - \psi} \Rightarrow \\ \ln\left(\frac{C^*_{\varepsilon 2} - 1}{C_{\varepsilon 2} - 1}\right) &= \ln\left(\frac{C_{\varepsilon 2} - \psi}{C_{\varepsilon 2} - 1}\right)\end{aligned} \tag{14}$$

By using the expression for $C^*_{\varepsilon 2}$ in Eq. 5 (with $f_2 = 1$), and ensuring that $0 < f_k \leq 1$ we finally get

$$f_k = \max\left[0, \min\left(1, 1 - \frac{\psi - 1}{C_{\varepsilon 2} - C_{\varepsilon 1}}\right)\right] \tag{15}$$

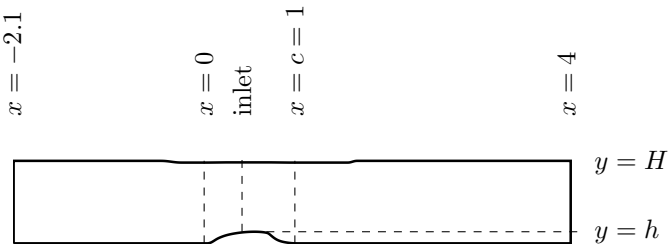

Figure 1: The geometry of the hump.

3 Results

The new formulation of f_k is evaluated and compared with $k - \varepsilon$ DES in two test cases, fully developed channel flow and the hump flow, see Fig. 1.

Channel flow

[1] ε is independent of f_k provided that no dissipation is resolved, which corresponds to $f_\varepsilon = 1$

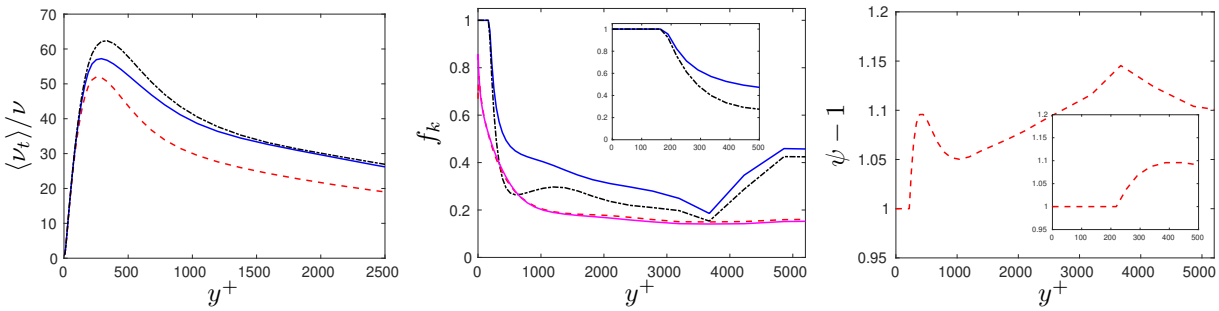

(a) Turbulent viscosity. ——: PANS; – – –: DES; –·–·–: PITM.

(b) ——: f_k, PANS; –·–·–: f_k: PITM; – – –: $f_{k,obs}$: PANS; ——: $f_{k,obs}$: PITM (see Eq. 16).

(c) ψ for DES.

Figure 3: Channel flow. Viscosity, f_k and ψ. $Re_\tau = 5\,200$.

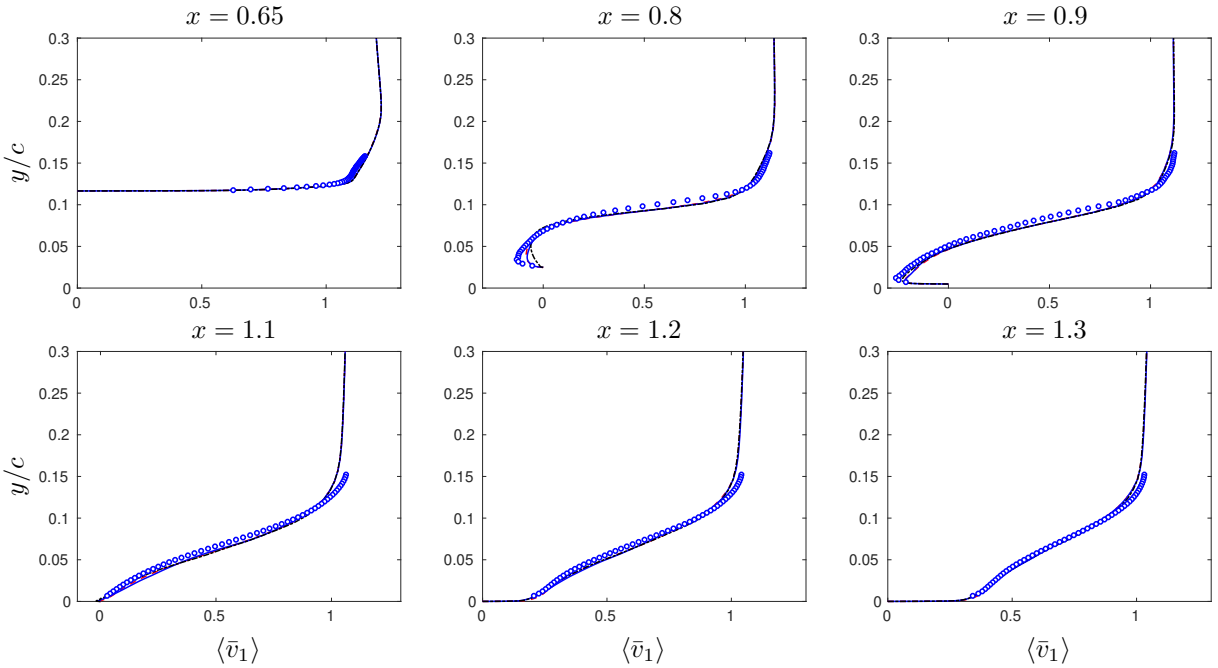

Figure 5: Hump flow. Velocities. ——: PANS; – – –: DES; –·–·–: PITM. Markers: Experiments.

The Reynolds number is defined as $Re_\tau = u_\tau \delta / \nu = 5\,200$ where δ denotes half channel height. The streamwise, wall-normal and spanwise directions are denoted by x, y and z, respectively. The size of the domain is $x_{max} = 3.2$, $y_{max} = 2$ and $z_{max} = 1.6$. The mesh has $32 \times 96 \times 32$ cells in the $x - y - z$ directions.

Figure 2 presents the velocity and the turbulent kinetic energy profiles. As can be seen, all velocity profiles exhibit a small bump near $y^+ = 1000$; otherwise they agree well with the DNS profile. The predicted turbulent kinetic energies with PANS and PITM agree well with DNS for $y^+ \gtrsim 500$ whereas DES gives slightly too small a value. Also the modeled turbulent kinetic energy is smaller for DES than for PITM/PANS. The reason they differ is that the assumption of homogeneous turbulence made when deriving Eq. 15 is not satisfied.

Figure 3 shows the turbulent viscosity, f_k and ψ. The turbulent viscosity is smaller for DES than for PANS/PITM which is in line with the smaller modeled turbulent kinetic energy in Fig. 2b. The peak in turbulent viscosity is lower with PANS than with PITM because the turbulent diffusion in the PANS model is much larger due to the small turbulent Prandtl numbers in the k and ε equations. Figures 3b and 3c show that the PANS/PITM and DES models switch from RANS to LES at the same location ($y^+ \simeq 200$, see insets). The observed f_k

$$f_{k,obs} = \langle k \rangle / (\langle k \rangle + k_{res}) \qquad (16)$$

is much smaller than the prescribed f_k, see Fig. 3b.

Hump flow

The Reynolds number of the hump flow is $Re_c = 936\,000$, based on the hump length, $c = 1$, and the inlet mean velocity at the centerline, $U_{in,c}$.

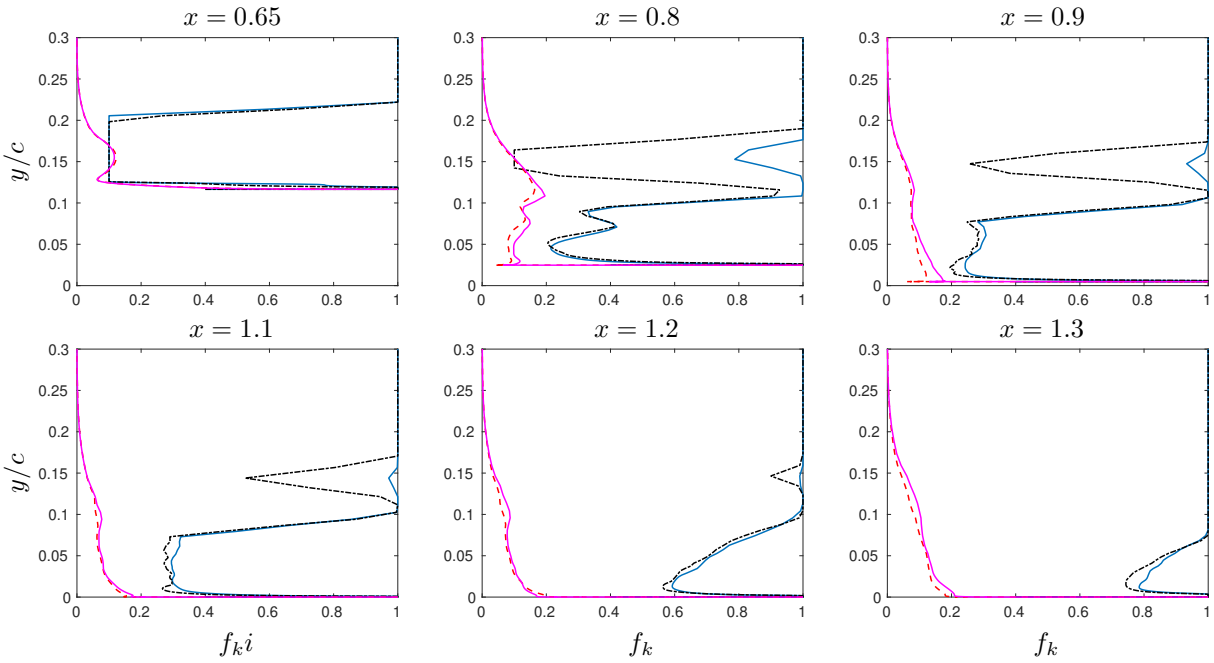

Figure 6: Hump flow. f_k. ▬: PANS; ▬·▬: PITM; ▬: $f_{k,obs}$: PANS; ▬: $f_{k,obs}$: PITM (see Eq. 16).

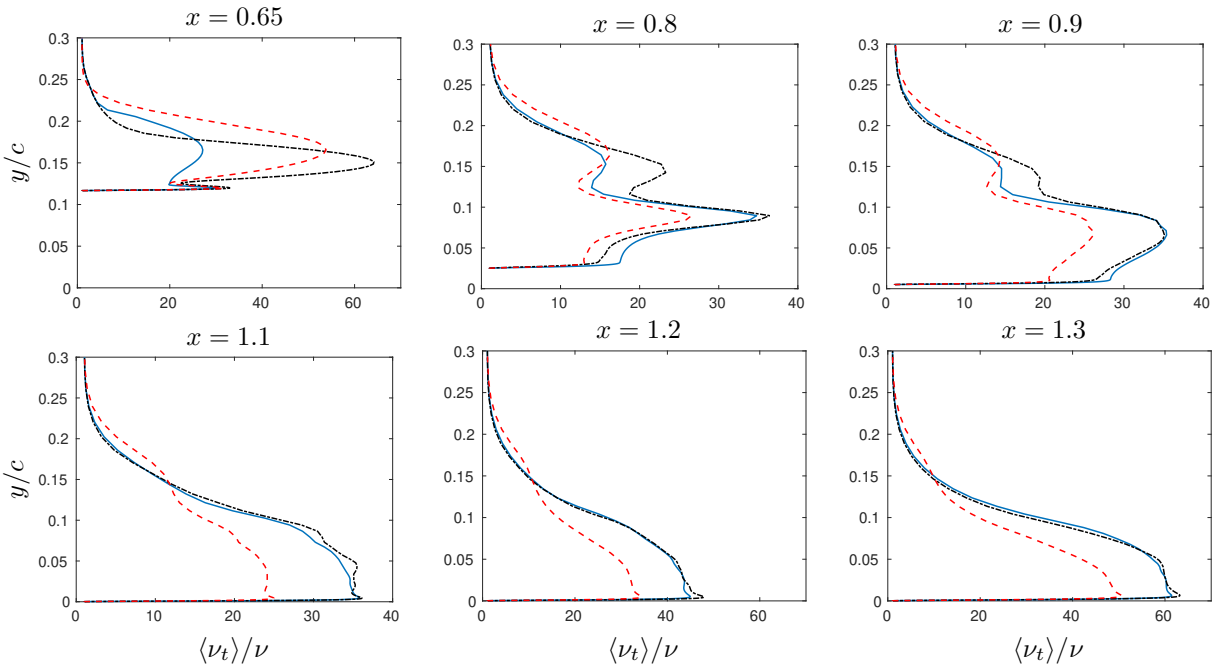

Figure 7: Hump flow. Turbulent viscosity. ▬: PANS; ▬: DES; ▬·▬: PITM.

In the present simulations, the value of ρ, c and $U_{in,c}$ have been set to unity. The configuration is given in Fig. 1. Experiments were conducted by Greenblatt et al. (2004, 2005). The maximum height of the hump, h, and the channel height, H, are given by $H = 0.91$ and $h = 0.128$, respectively. The mesh has $304 \times 108 \times 32$ cells with $Z_{max} = 0.2$ and it is taken from the NASA workshop.[2] The inlet is located at $x = 0.5$ and the outlet at $x = 4.0$.

The inlet conditions (U, V, k and ε) are taken from a 2D RANS simulation using the AKN $k-\varepsilon$ turbulence model (Abe et al. 1994) coupled to the EARSM model (Wallin & Johansson 2000). Synthetic isotropic fluctuations are superimposed on the 2D RANS velocity field. The synthetic fluctuations are scaled with the RANS shear stress profile. To reduce the inlet k, prescribed from 2D RANS, a commutation term $\partial f_k / \partial x$ is used. In the DES simulations, a term corresponding to a reduction of f_k from 1 to 0.4 at the inlet is employed. For more detail on inlet synthetic fluctuations and the commutation term, see Davidson (2016).

[2] https://turbmodels.larc.nasa.gov/nasahump_val.html

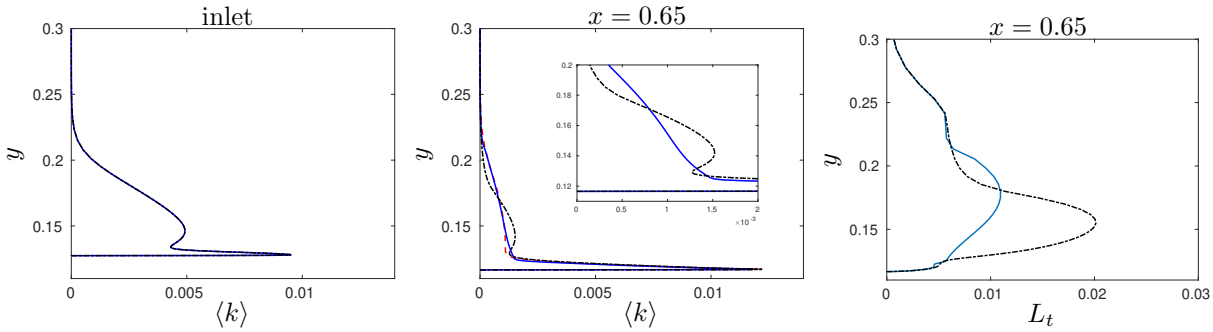

(a) Modelled turbulent kinetic energy.

(b) Modelled turbulent kinetic energy.

(c) Modelled turbulent length scale, $L_t = \langle k \rangle^{3/2}/\langle \varepsilon \rangle$.

Figure 8: Hump flow. Modeled turbulence. ——: PANS; —·—·—: PITM.

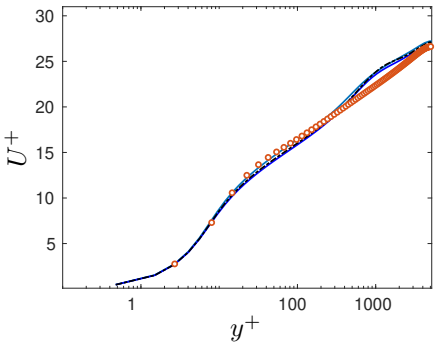

(a) Velocity. ——: PANS; – – –: DES; —·—·—: PITM.

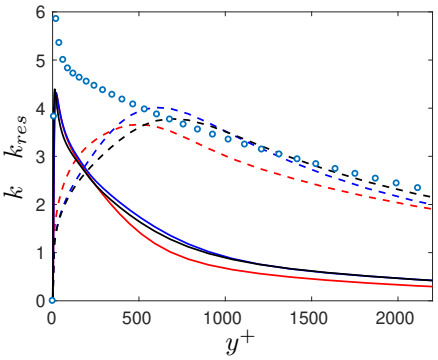

(b) Turbulent kinetic energy. Top: resolved; bottom: modeled; blue lines: PANS; red lines: DES; black lines: PITM..

Figure 2: Channel flow. $Re_\tau = 5\,200$. Markers: DNS

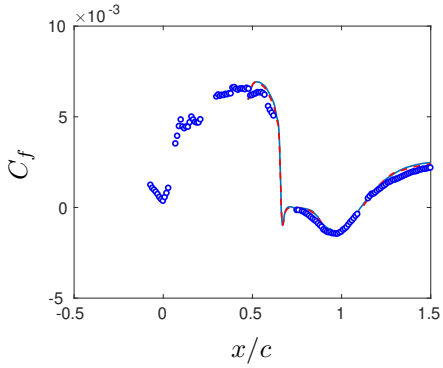

Figure 4: Hump flow. Skinfriction. ——: PANS; – – –: DES; —·—·—: PITM. Markers: Experiments.

Figures 4 and 5 compare predictions with experiments and, as can be seen, the agreement is very good for all three models. The predicted skinfrictions show a small bump near the inlet, and the reason is (at least partly) that a different RANS turbulence model (EARSM) was used in the 2D RANS simulations than the underlying RANS model in the PANS/PITM/DES simulations. The strength of the backflow is slightly underpredicted by all models at $x = 0.8$ (the PITM model gives the weakest backflow) compared to experiments.

Figure 6 presents f_k for PANS and PITM. f_k for PANS and PITM are very similar in the boundary layer and in the recirculating region. But in the region above the recirculating region for $0.8 \leq x \leq 1.1$, f_k is much smaller for PITM than for PANS. The reason is that the RANS inlet profile of k has a secondary peak at $y = 0.15$, see Fig. 8a. With PITM, this peak is transported downstream to $x = 0.65$ (Fig. 8b) and gives a large peak in the turbulent lengthscale at $x = 0.65$, see Fig. 8c. The large turbulent lengthscale results in a large ψ (see Eq. 11), which gives a small f_k (see Eq. 15). PANS, on the other hand, has no problems with the secondary peak of k at the inlet. Thanks to the large diffusion in k and ε (recall that the turbulent Prandtl numbers in the k and ε

equations are divided with f_k^2), the peak is quickly smoothed out. The secondary peak in k has disappeared at $x = 0.65$, see Fig. 8b. However, it should be noted that the small f_k in the PITM model has negligible influence on the mean flow. In the outer part of the flow, f_k is equal to one since the resolved turbulence is zero.

The observed f_k (see Eq. 16) is also shown in Fig. 6. It is fairly similar to f_k in the boundary layer at $x = 0.65$ but further downstream in the recirculation region the observed f_k is approximately half as large as the prescribed f_k. In the attached flow region the observed f_k is much smaller than the prescribed f_k.

Figure 7 shows the turbulent viscosity for the three models. As in the channel flow, the turbulent viscosity is smaller for DES than PANS/PITM. The peak for PITM at $x = 065$, $y = 0.15$ corresponds to the peak in k (Fig. 8b).

4 Concluding remarks

A new formulation for prescribing f_k has been presented. It gives good results and according to the experience of the first author, it is better than any other form of f_k presented in the literature. So what is the advantage of using PANS/PITM instead of DES? One advantage is that PANS and PITM have a much stronger theoretical foundation than DES. The former models are rigorously derived (but quite different derivations!) whereas DES is an ad-hoc (but very successful) modification of a RANS model. Another advantage of PANS/PITM is that the modified partition between modeled and resolved turbulence due to non-uniform grids can be accounted for by adding a term in the k and momentum equations based on the gradient of f_k (Girimaji & Wallin 2013, Davidson 2016). Future work will focus on a thorough theoretical derivation of the relationship between f_k and the grid step, by accounting for inhomogeneity.

References

Abe, K., Kondoh, T. & Nagano, Y. (1994), 'A new turbulence model for predicting fluid flow and heat transfer in separating and reattaching flows - 1. Flow field calculations', *Int. J. Heat Mass Transfer* **37**(1), 139–151.

Basara, B., Krajnović, S., Girimaji, S. & Pavlović, Z. (2011), 'Near-wall formulation of the Partially Averaged Navier Stokes turbulence model', *AIAA Journal* **49**(12), 2627–2636.

Chaouat, B. & Schiestel, R. (2005), 'A new partially integrated transport model for subgrid-scale stresses and dissipation rate for turbulent developing flows', *Physics of Fluids* **17**(065106).

Davidson, L. (2016), 'Zonal PANS: evaluation of different treatments of the RANS-LES interface', *Journal of Turbulence* **17**(3), 274–307. **URL:** *http://dx.doi.org/10.1080/14685248.2015.1093637*

Foroutan, H. & Yavuzkurt, S. (2014), 'A partially-averaged Navier-Stokes model for the simulation of turbulent swirling flow with vortex breakdown', *International Journal of Heat and Fluid Flow* **50**, 402–416.

Friess, C., Manceau, R. & Gatski, T. (2015), 'Toward an equivalence criterion for hybrid RANS/LES methods', *International Journal of Heat and Fluid Flow* **122**, 233–246.

Girimaji, S. S. (2006), 'Partially-averaged Navier-Stokes model for turbulence: A Reynolds-averaged Navier-Stokes to direct numerical simulation bridging method', *ASME Journal of Applied Mechanics* **73**(2), 413–421.

Girimaji, S. S. & Abdol-Hamid, K. S. (2005), 'Partially-Averaged Navier-Stokes model for turbulence: Implementation and Validation', AIAA paper 2005-0502, Reno, N.V.

Girimaji, S. S. & Wallin, S. (2013), 'Closure modeling in bridging regions of variable-resolution (VR) turbulence computations', *Journal of Turbulence* **14**(1), 72 – 98.

Greenblatt, D., Paschal, K. B., Yao, C.-S. & Harris, J. (2005), 'A separation control CFD validation test case Part 1: Zero efflux oscillatory blowing', AIAA-2005-0485.

Greenblatt, D., Paschal, K. B., Yao, C.-S., Harris, J., Schaeffler, N. W. & Washburn, A. E. (2004), 'A separation control CFD validation test case. Part 1: Baseline & steady suction', AIAA-2004-2220.

Kenjeres, S. & Hanjalic, K. (2006), 'LES, T-RANS and hybrid simulations of thermal convection at high ra numbers', *International Journal of Heat and Fluid Flow* **27**, 800–810.

Schiestel, R. & Dejoan, A. (2005), 'Towards a new partially integrated transport model for coarse grid and unsteady turbulent flow simulations', *Theoretical and Computational Fluid Dynamics* **18**(6), 443–468.

Wallin, S. & Johansson, A. V. (2000), 'A new explicit algebraic Reynolds stress model for incompressible and compressible turbulent flows', *Journal of Fluid Mechanics* **403**, 89–132.